AIMS Materials Science, 6(5): 730–747.
DOI: 10.3934/matersci.2019.5.730
Received: 31 May 2019
Accepted: 11 August 2019
Published: 16 August 2019

http://www.aimspress.com/journal/Materials

Research article

Characterization and enhancement of physico-mechanical properties of glass ionomer cement by incorporating a novel nano zirconia silica hydroxyapatite composite synthesized via sol-gel

Arbaz Sajjad[1], Wan Zaripah Wan Bakar[2,*], Dasmawati Mohamad[3], Thirumulu Ponnuraj Kannan[1]

[1] School of Dental Sciences (PPSG), Universiti Sains Malaysia (Health Campus), kubang Kerian, Malaysia
[2] Conservative Dentistry Unit, School of Dental Sciences (PPSG), Universiti Sains Malaysia (Health Campus), kubang Kerian, Malaysia
[3] Dental Materials Department, School of Dental Sciences (PPSG), Universiti Sains Malaysia (Health Campus), kubang Kerian, Malaysia

* **Correspondence:** Email: wzaripah@usm.my; Tel: +60199091968.

Abstract: In restorative dentistry, there has been a growing shift towards using nanoparticles dispersed in the polymer matrix to improve properties of dental restorative materials. A new nano zirconia–silica–hydroxyapatite (nanoZrO_2–SiO_2–HA) was synthesized by one-pot synthesis and characterized using transmission electron microscopy (TEM), scanning electron microscopy (SEM), fourier transform infrared spectroscopy (FTIR), energy dispersive X-ray (EDX) and dot mapping. The effect of addition of nanoZrO_2–SiO_2–HA to the conventional GIC (cGIC) on the compressive strength, flexural strength and surface roughness was also evaluated. The characterization studies confirmed that all particles were in the nanoscale range with spherical zirconia and silica particles embedded in the voids between rod-shaped HA crystallites. The nano particles were evenly and homogenously dispersed throughout the sample with high density patterns visible for zirconia, calcium and phosphorus. The incorporation of 5% nanoZrO_2–SiO_2–HA has resulted in considerable improvement in the compressive and flexural strengths of cGIC. The GIC 5% nanoZrO_2–SiO_2–HA exhibited an increase in compressive (144.12 ± 13.88 MPa) and flexural strength (18.12 ± 2.33 MPa)

over cGIC which was statistically significant ($p \leq 0.05$). It also demonstrated surface roughness profile (0.15 ± 0.029 μm) similar to that of cGIC (0.15 ± 0.019 μm). Therefore, the nanoZrO_2–SiO_2–HA can be a promising filler for GIC to be used as restorative dental material in high stress bearing areas.

Keywords: glass ionomer cement; nanomaterials; mechanical properties; characterization; zirconia

1. Introduction

Many restorative materials have been used in dentistry over the decades. There is now a trend towards the use of tooth-colored restorative materials such as conventional glass ionomer cement (cGIC) and composite resins. Composite resins are, however, often considered unsuitable for special needs and pediatric patients due to the difficulty of isolation and moisture contamination during placement of the restoration [1]. On the other hand, glass ionomer cements are do not require such stringent moisture control and isolation protocols [2,3]. They were first introduced in dentistry by Wilson et al. at the Laboratory of the Government Chemist in 1969 [4,5].

GIC is the generic name for a group of classifying materials originally produced from alumino-silicate polyacrylates [6,7]. The powder of the ionomer glass is manufactured by fusion of its main components (SiO_2, Al_2O_3 and CaF_2) at a temperature between 1100 and 1500 ℃ to form a homogeneous fluoro-aluminosilicate glass [8,9]. Silica and alumina are responsible for the mechanical strength of the material, while calcium fluoride contributes to the F ions release at the surrounding media [10,11].

As aqueous polyelectrolyte systems, GICs are known for their relative ease of use, chemical bonding to tooth substrate, fluoride ion release and recharge, low coefficient of thermal expansion and acceptable aesthetic quality [12]. GIC is also found to be biocompatible with pulp tissue and with primary cultures of bone cells. In the clinic, however, the use of GIC is limited due to its relatively inferior mechanical properties and sensitivity to initial desiccation and moisture [13–15].

To expand the usage of cGIC, especially for restoration of adult teeth and for anterior teeth restorations, the physical, mechanical and aesthetic properties must be improved. The polymeric substrate of these ionomeric cements act as a vehicle or carrier for different organic and inorganic fillers or additives. Glass ionomers have already distinguished themselves as unique restorative materials possessing the potential for remineralisation and antimicrobial action owing to their fluoride uptake and elusion ability. As a result of this unique ability, GICs have potentially been employed as templates for releasing other active antimicrobial components, thereby, further expanding their use as a restorative material for deciduous teeth and in atraumatic restorative therapy (ART) [16].

The earliest attempt has been reported by Simmons in 1983 via simple addition of silver amalgam alloy powder to GIC powder and subsequently, McLean and Gasser fused and sintered amalgam powders to basic glass particle [17,18]. The resulting cermet particles exhibited strong bonding between the metallic and glass particles. However, these modifications were still not enough

for GICs to be used as a posterior restorative material [19,20]. Metal powders [21–25], reactive glass fibres [26,27] and other non-reactive fillers have been evaluated as potential reinforcement phases in order to improve the mechanical properties of GICs without compromising their adhesive and fluoride release properties. In one such study, researchers added micron size hydroxyapatite (HA: $Ca_{10}(PO_4)_6OH_2$) to cGIC resulting in improved biological properties of GIC [28]. Later, Yap et al. reported that the addition of HA enhanced the hardness of GIC [29]. Hydroxyapatite is an integral part of enamel and dentine with an ability to remineralize initial incipient caries and improve the bond strength to dentine [2,30].

In restorative dentistry, there has also been a growing shift towards using nanoparticles to improve properties of cGICs [31]. In the last decade, nanoscale HA [32,33], combination of HA–silica (SiO_2) [34,35] have been successfully used to improve GICs. Recently, nanophases of zirconia (ZrO_2) or a combination of HA–ZrO_2 [36–38] have been incorporated in attempts to strengthen GIC with enhanced outcomes. Zirconium and its oxide, due to their good dimensional stability and toughness (on the same order as stainless-steel alloys), have been used widely for the toughening and strengthening of brittle HA bio glasses in biomedical applications [39]. Furthermore, ZrO_2 has been used in fabrication of high strength core for dental implants [40]. Another more recent study was done to evaluate the microhardness of a HA–SiO_2–ZrO_2 incorporated GIC with some encouraging results [41].

However, there is still dearth of information on the assessment of physico-mechanical properties of nanoZrO_2–SiO_2–HA GIC hybrid in terms of compressive strength (CS), flexural strength (FS) and surface roughness (SR). Therefore, the aim of the present study was to evaluate the effectiveness of a novel nanoZrO_2–SiO_2–HA reinforcement phase on the physico-mechanical properties of cGIC. The nano powder was synthesized and characterized morphologically and qualitatively prior to the evaluation of CS, FS and SR of the GIC nanoZrO_2–SiO_2–HA hybrid material. The null hypothesis tested was that the addition of ZrO_2–SiO_2–HA to the cGIC does not improved its physico-mechanical properties.

2. Materials and methods

2.1. Materials

The alumino-silicate glasses and the polyacids used in the research study were from commercially available Fuji IX® (GC, Tokyo; Japan). All the other chemicals and materials were of analytical grade and used as received from the manufacturer. Tetraethyl orthosilicate (TEOS, >99%), ammonia (NH_3, 25%) and calcium hydroxide ($Ca(OH)_2$, >98%) were obtained from Merck Serono Pvt. NSW, Australia. Phosphoric acid (H_3PO_4, >99%), and ethanol (C_2H_5OH, >99%) were procured from Sigma-Aldrich Co. LLC, MO, USA, and Zr nanopowder (ZrO_2, >99%) was from US Research Nanomaterials Inc., TX, USA.

2.2. Synthesis of nanoZrO$_2$–SiO$_2$–HA

The nanoZrO$_2$–SiO$_2$–HA was synthesized using a modification of the sol-gel technique [42] described by Ab Rahman et al. [41]. Initially, Ca(OH)$_2$ was dissolved in distilled water using a magnetic stirrer until a suspension was formed. After this, a stoichiometric amount (i.e., Ca/P molar ratio of 1.67) of H_3PO_4 (0.075 M) held in a burette was added drop wise to the suspension and the pH of the suspension was adjusted by adding ammonia till it was stabilized in the range of 11–12. The resulting suspension was stirred continuously for 48 h. Then, a quantity of 5 mL of TEOS and 25 wt% ZrO_2 dissolved in C_2H_5OH was added drop wise. C_2H_5OH was mixed with TEOS because it is immiscible in water, but dissolves easily in C_2H_5OH. Hence, the mixing greatly affects the homogeneity of TEOS in the reaction. Finally, the sol was stirred for an additional 12 h and then centrifuged (Centrifuge 5702, Eppendorf®, Hamburg; Germany), washed with C_2H_5OH, freeze dried (ScanVAc CoolSafe, LaboGene ApS; Lynge) and calcined (WiseTherm®, Witeg Lab. GmbH; Germany) at 600 ℃ for 1 h.

2.3. Characterization of nanoZrO$_2$–SiO$_2$–HA nanopowder

The morphology and microstructure of the samples was studied by using a fully analytical energy filtered transmission electron microscopy (EFTEM) with an acceleration voltage of 120 kV and objective lenses with resolution point of 0.34 nm (Zeiss Libra 120 plus). Dilute dispersion of 100 mg of nano powder was washed in 3 mL of ethanol and was subjected to ultrasonication for 10 min to disperse the nano particles and to obtain a homogeneous suspension. One drop of this suspension was carefully placed with the help of a pipette on a 2.3 mm carbon-coated copper grid with a thickness of 10–20 nm.

The microstructure of the nanoZrO$_2$–SiO$_2$–HA dehydrated powder was also observed under scanning electron microscopy (SEM, Quanta™FEG, ThermoFisher©, OR; USA). Prior to evaluation, each powder specimen was coated with gold using a sputter coater (Desk-II, Denton Vacuum Inc., NJ; USA) at a gas pressure of ~50 mTorr, and ~40 mA current. The coating time required was 180 s. Energy dispersive X-ray analyzer (EDX, Rontec; Germany) which was directly connected to SEM was used to investigate semi quantitatively the chemical composition of the nanoZrO$_2$–SiO$_2$–HA.

In addition, Fourier transform infrared spectra (Spectrum Two™ FTIR, PerkinElmer, MA; USA) of the GIC nanoZrO$_2$–SiO$_2$–HA powder was measured in the spectral range of 400–4000 cm^{-1}. The standard spectral resolution of the instrument was between 0.16 and 0.5 cm^{-1} suitable for most applications.

2.4. Fabrication of GIC nanoZrO$_2$–SiO$_2$–HA hybrid samples

Conventional GIC, Fuji IX® was used as control and base material. The nanoZrO$_2$–SiO$_2$–HA powder was added at varying percentage of 3%, 5%, 7% and 9% by weight into the cGIC to prepare a total of four experimental groups. The mixture was then ground manually using a pestle and mortar in a control grinding process for about 10 min. All the samples (cGIC and GIC nanoZrO$_2$–SiO$_2$–HA) were prepared by mixing with Fuji IX-liquid at the recommended powder/liquid ratio (P/L) of 3.6.

The physico-mechanical properties evaluated were compressive strength, flexural strength and surface roughness after 24 h of setting.

2.4.1. Compressive strength testing

Cylindrical samples measuring 4 mm × 6 mm were prepared in stainless-steel split mould following the procedures outlined in ISO 9917-1: 2007. The moulds were coated with a thin layer of cocoa butter provided by the manufacturer of Fuji IX prior to filling the moulds to facilitate the easy retrieval of the set samples. They were then filled with the material and covered with polyester strips and glass slides and gently pressed by hand to remove air bubbles from uncured cement paste. The split mould was carefully disassembled after 30 min and the samples were gently retrieved by hand from the moulds and conditioned in distilled water at 37 ℃ for 24 h. Then, each sample was placed with the flat ends between the platens of a universal testing machine (AG-X plus 20 KN, Shimadzu Corp.; Japan) and a compressive load was applied along the long axis of the sample at a crosshead speed of 1 mm/min until the sample fractured. The compressive strength (CS) was calculated in mega pascals (MPa) using the following equation: $CS = 4P/\pi d^2$, where P is the load at fracture (N), and d is the diameter (mm) of the cylindrical sample and π is Pi which has a numerical constant of 3.14.

2.4.2. Flexural strength testing

Beam-shaped samples measuring 3 mm × 3 mm × 25 mm were prepared in a stainless-steel split mould following the procedures outlined in ISO 9917-2: 2007 and as aforementioned. Samples were kept in 100% humidity at 37 ℃ for 50 min before being immersed in distilled water and stored for 23 h at 37 ℃ [43]. Then, they were subjected to a three-point bending test in a universal testing machine (AG-X plus 20 KN, Shimadzu; Japan) at a crosshead speed of 0.5 mm/min with a 20 mm span or at a rate of loading of 50 ± 16 N/min and the flexural strength (FS) was recorded.

2.4.3. Surface roughness evaluation

A polytetrafluorethylene mould (5 mm diameter × 2 mm deep) was used to prepare how many samples according to the procedure outlined before. The prepared samples were then stored at 100% relative humidity for 24 h. Only a polyester strip and a glass slide were used with the intention of obtaining a smooth surface. Any form of additional polishing can lead to an increase in surface roughness (SR) and hence no polishing of the samples was carried out [44].

Each sample was blot dried and subjected to SR testing using a profilometer (Surfcom Flex, Accretech, Tokyo Seimitsu Co. Ltd.; Japan) and the value (Ra) obtained was in μm. To measure the roughness profile value, the diamond stylus (5 μm tip radius) was moved across the surface under a constant load of 4 mN. Five measurements passing through the center of the sample were performed and the average Ra taken. The cut-off value for surface roughness will be 0.8 mm based on mathematical cut-off filters in-built in the processor unit.

2.4.4. Statistical analysis

The data was analysed using using SPSS version 22.0 (SPSS Inc., Chicago, IL; USA). Numerical data was tabulated and presented as mean ± SD based on their normality distribution. A $p \leq 0.05$ was considered as statistically significant. One-way analysis of variance (ANOVA) was performed to determine whether *p*-value was statistically significant, and a post-hoc Tukey's HSD multiple range test was used to determine which experimental groups were statistically different from one another in the evaluation of *CS*, *FS* and *SR*.

3. Results and discussion

3.1. Characterization interpretations

3.1.1. FTIR spectra analysis of GIC nanoZrO_2–SiO_2–HA hybrid

FTIR absorption spectra (Spectrum Two™ FTIR, PerkinElmer, MA; USA) of the GIC nanoZrO_2–SiO_2–HA hybrid containing 3 to 9% of nanoZrO_2–SiO_2–HA filler was measured in the spectral range of 400–4000 cm^{-1}. The standard spectral resolution of the instrument was between 0.16 and 0.5 cm^{-1} suitable for most applications.

FTIR analysis shows some variations in adsorption peaks of the GIC nanoZrO_2–SiO_2–HA hybrid material when compared to the FTIR of nanoZrO_2–SiO_2–HA nanopowder [41] (Figure 1). The band at 3436.60- is due to ν_2 bending mode of absorbed water OH stretching vibration confirming the presence of alcohols and phenols [34,41,45]. The band at 1709.51 is due to stretching vibration of carboxyl group of ketones or quinone. This confirms ν_3 stretching vibration of PO_4^{3-}. The peaks at 964.41, 1041.56 and 1093.64 observed in the FTIR spectra of nanoZrO_2–SiO_2–HA [41] (representing the bending mode of PO_4^{3-} and the stretching vibration of Si–O, Zr–O) are replaced by a prominent peak at 1034.28 which becomes a bit broad in the GIC nanoZrO_2–SiO_2–HA hybrid but is otherwise stable in position. It arises due to symmetric and asymmetric stretching of Si–O–Si, i.e., with the addition of Zr it increases the distance of Si–O [34,41,46]. It specifies the Zr–O–Si bond formation and is because of the large ionic radius of Zr [38,47].

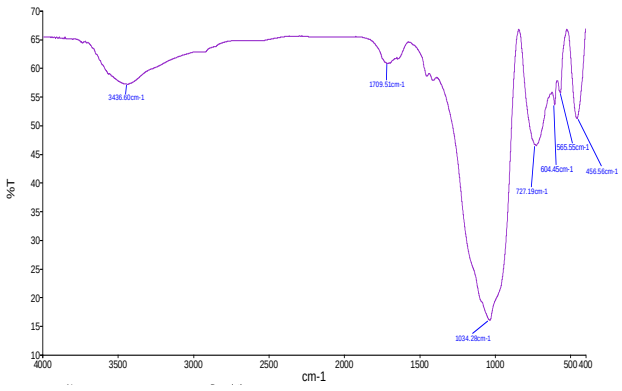

Figure 1. FTIR spectra of GIC nanoZrO_2–SiO_2–HA hybrid material.

The small peak at 731.02 seen in the FTIR spectra of nanoZrO_2–SiO_2–HA [41] is replaced by a prominent peak at 727.19 that arises due to CaF_2; this peak might also be due the presence of θ-Al_2O_3. A new peak 456.56 appears due to the bending vibration of Si–O–Si, $AlPO_4$ and α-Al_2O_3. These results indicate some molecular interaction presented between the nanoZrO_2–SiO_2–HA and GIC in the composite.

3.1.2. TEM evaluation

Comparative morphologies of nanoZrO_2, nanoSiO_2 and HA prepared by the modified sol-gel technique [34,41,43], as observed under EFTEM in a 200 nm micrograph are shown in Figure 2. The image reveals a narrow size and shape distribution in the morphology of the particles with roughly low agglomeration and aggregation.

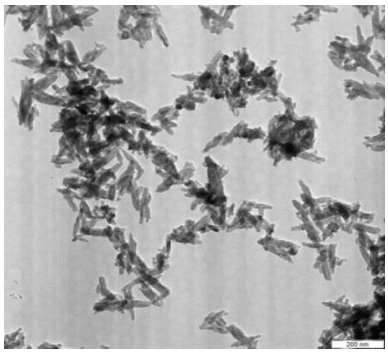

Figure 2. TEM micrograph of nanoZrO_2–SiO_2–HA at low magnification (40000×)

The 100 nm micrograph confirm that the asymmetrically elongated rod like structures are indeed HA crystallites (Figure 3a), which has been documented in previous studies [35,36] and apart from the elongated rod shaped HA structures, smaller spherical structures embedded between and along the elongated HA are the silica particles [34,56,58]. These are also accompanied with oval to spherical slightly larger and darker structures which are most likely the nanoZrO_2 particles (Figure 3a,b) and these observations are in agreement with findings of a previous study [38]. These micrographs confirmed our assumption that all the powder particles were in or close to the nano scale range with the elongated HA measured to a mean length of 114 nm with SiO_2 having a mean size of approximately 18 nm (Figure 3a, Inset). These observations were in agreement with previously published literature [34,41,42,56]. The nanoZrO_2 had a mean size of 39 nm which confirms that the particles are indeed ZrO_2 as the commercially supplied ZrO_2 used in the one-pot synthesis was of the dimension of 40 nm and these dimensions are similar to many published studies [37,38,41]. The overall smaller particle sizes were attributed to the modified one-pot synthesis technique and the prolonged freeze drying. Slowing the rate at which ammonia is fed resulted in smaller ZrO_2 and SiO_2 nanoparticles and freeze drying produced mesoporous crystallites with high surface area.

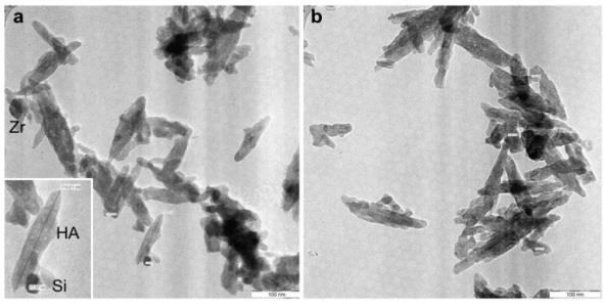

Figure 3. TEM micrograph of nanoZrO_2–SiO_2–HA at high magnification (60000×) at two different locations (a) and (b), Figure 3(a) inset shows the close up microstructure of HA and Si.

There was presumably a homogenous mix of the rod-shaped HA, spherical ZrO_2 and SiO_2 particles in the nano powder. Therefore, it can be inferred that the morphology of the nanoZrO_2–SiO_2–HA powder consists of a mixture of spherical ZrO_2, SiO_2 particles embedded in the voids or spaces between rod-shaped HA.

3.1.3. SEM evaluation

SEM micrographs of nanoZrO_2–SiO_2–HA powder in Figure 4a,b clearly reveal that nano hybrid powder is a mixture of elongated rod-shaped structures which is HA crystallites, smaller spherical powder shaped structures which are SiO_2 particles in close proximity of which are the spherical slightly larger and whiter nanoZrO_2 particles. These observations are in line with many of the previously reported literature [34,35,38,57]. The SEM images also confirm that nanoSiO_2 and nanoZrO_2 have occupied the spaces present between HA rods compacting the nano powder and forming a denser and stronger nanoZrO_2–SiO_2–HA powder [36,41,43,59]. The higher magnification (200000×) SEM micrograph (Figure 4b) reveals that the nanoHA rods have a rough outer texture which suggests that they may be covered by very fine SiO_2 and probably ZrO_2 residue. Similar conclusions have been recorded by authors in another study [43].

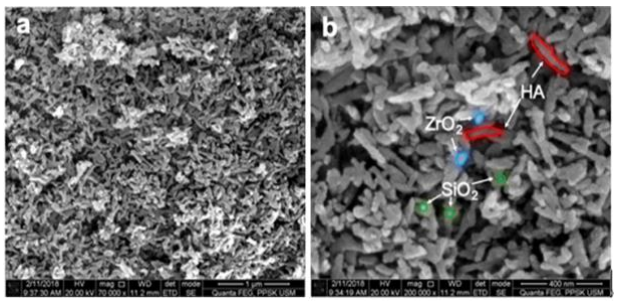

Figure 4. SEM micrograph of nanoZrO_2–SiO_2–HA at (a) low magnification (70000×) and (b) high magnification (200000×).

3.1.4. EDX and dot mapping analysis

Energy dispersive X-ray results in Figure 5 shows that the main elements present in the nanoZrO_2–SiO_2–HA powder are Ca, P, Zr, Si and O. A total of 4 iterations were done and peaks possibly omitted were at 9.703, 11.508 keV. L-alpha line of Ca was present while K-alpha lines of Si, O, P and Ca are observed. Thus, it is affirmed that a nanoZrO_2–SiO_2–HA nano composite is formed after analyzing the quantative presence of Ca, P and Si in the EDX spectrum.

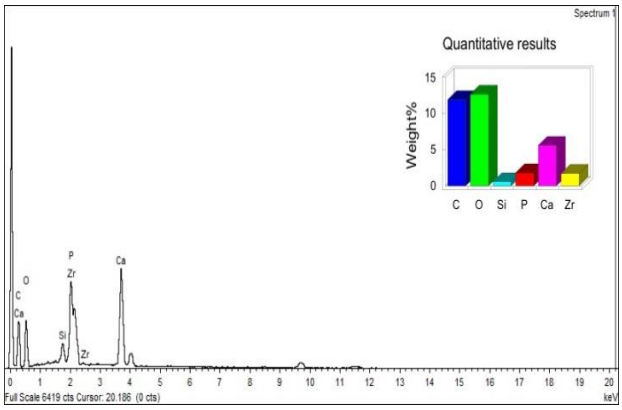

Figure 5. EDX spectrum of nanoZrO_2–SiO_2–HA.

It is possible to analyse the spatial distribution and density of Zr, Si, HA in the powder by performing a dot mapping using EDX. Figure 6 shows the SEM dot mapping characteristics for (a) Zr, (b) Ca, (c) P and (d) Si. All of these elements were evenly and homogenously dispersed throughout the sample scan area with high density patterns visible for Zr, Ca followed by P without any evident of clumping or aggregation [41]. Si was the least dense with uniform distribution which is in accordance with the low quantity of TEOS (5 mL) used in the one-pot synthesis.

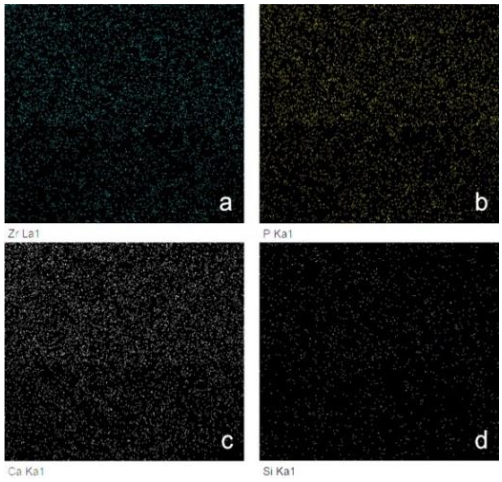

Figure 6. SEM dot mapping of (a) Zr, (b) P, (c) Ca, (d) Si of nanoZrO_2–SiO_2–HA.

3.2. Evaluation of physico-mechanical properties

Mechanical properties are very important for a dental restorative material. In order to obtain maximum service, these materials should withstand the forces generated during mastication [60]. The stability of a solid material under the applied force is determined by the nature of the material and atomic bond strengths. Materials used in restorative dentistry should have sufficient strength to withstand the complex forces that repeatedly can arise from mastication during the chewing process. The average force that is observed in chewing is about 200–400 N [61].

Physical properties especially surface roughness (SR) of restorative materials in the oral environment is an important criterion to predict their clinical deterioration. Surface characteristics of GIC restorations are particularly of concern because rough surfaces are more prone to faster bacterial colonization and plaque maturation, thereby increasing the risk of caries [62] ultimately leading to staining and poorer aesthetics. In addition, an increase in SR might indicate material deterioration [63–65].

3.2.1. Compressive strength evaluation

Compressive strength is useful for comparing materials that are brittle and generally weak (such as GICs) in tension [66]. The compressive strength of a material is defined as the maximum stress that the material can undergo without fracture. Compressive strength is widely used as a method of measuring the strength of GICs. Fuji IX Universal was selected as the control GIC because it is a widely popular commercially available cGIC and is recommended for this reason by WHO for ART [33]. Also, Fuji IX contains glass predominantly composed of SiO_2, AlO_3, CaF_2, Na_3AlF_6, and $AlPO_4$ in which the Ca is substituted with Sr without affecting the setting reaction of GIC. Therefore, the absence of Ca in the glass composition of Fuji IX was considered an advantage as it would not interfere with the characterization and quantitative assessment of Ca release characteristic from HA of the nanoZrO_2–SiO_2–HA powder. The similarity between HA and the chemical and skeletal structure of bone and teeth makes it an obvious candidate to expand the applications of GIC [67]. Similarly, high strength, fracture toughness and biocompatibility of ZrO_2 make it a valuable adjunct for overcoming the brittleness of HA [36,37,68,69].

Table 1 shows the CS of GIC nanoZrO_2–SiO_2–HA experimental groups and cGIC which were tested after being immersion in distilled water bath at 37 ℃ for 1 d. The data demonstrate that compared with the control, the GIC nanoZrO_2–SiO_2–HA groups exhibited considerably higher compressive strength ($p < 0.05$) for GIC 5% nanoZrO_2–SiO_2–HA group (144.12 ± 13.88 MPa). This finding is in agreement with previous results which reported the highest increase in CS for 4% GIC-HA as compared to Fuji IX [29]. The GIC 5% nanoZrO_2–SiO_2–HA exhibited a ~30% increase in CS over Fuji IX. These values were higher than the increase of ~18.42% reported by Moheet et al. [43] for GIC nanoHA–SiO_2 as well as the ~14% in CS of a GIC–HA material developed by Moshaverinia et al. [70]. This was probably due to the high ZrO_2 content (25%) of the nano powder. The results also exhibited a linear correlation up to 5 wt% addition of nanoZrO_2–SiO_2–HA powder to the GIC after which the CS values decreased. This could be due to the overcrowding of the nano filler at over 5 wt%, resulting in the disruption of the poly salt bridge formations in the GIC matrix.

It is postulated that the glass component of this hybrid GIC undergoes finely controlled micronization to achieve optimum particle size and characteristics [71]. In addition, the homogeneous and dense presence of ZrO_2 particles in the nano powder further reinforces and improves the mechanical properties of GIC as verified by SEM dot mapping scans. The nanoZrO_2–SiO_2–HA particles occupy the empty voids between the glass particles, thereby enhancing the packing density and acting as a reinforcement phase in the GIC composition [41,59].

Table 1. Compressive strength comparison between the various experimental groups.

Group	Comparison	Mean compressive strength ± SD (MPa)	*p*-value
Control (117.64 ± 16.40 MPa)	GIC 3% nanoZrO_2–SiO_2–HA	126.78 ± 9.369	0.215
	GIC 5% nanoZrO_2–SiO_2–HA	144.12 ± 13.88*	0.000
	GIC 7% nanoZrO_2–SiO_2–HA	133.84 ± 15.77*	0.003
	GIC 9% nanoZrO_2–SiO_2–HA	120.47 ± 8.59	0.964
GIC 3% nanoZrO_2–SiO_2–HA	GIC 5% nanoZrO_2–SiO_2–HA	144.12 ± 13.88*	0.001
	GIC 7% nanoZrO_2–SiO_2–HA	133.84 ± 15.77	0.471
	GIC 9% nanoZrO_2–SiO_2–HA	120.47 ± 8.59	0.583
GIC 5% nanoZrO_2–SiO_2–HA	GIC 7% nanoZrO_2–SiO_2–HA	133.84 ± 15.77	0.125
	GIC 9% nanoZrO_2–SiO_2–HA	120.47 ± 8.59*	0.000
GIC 7% nanoZrO_2–SiO_2–HA	GIC 9% nanoZrO_2–SiO_2–HA	120.47 ± 8.59*	0.020

*Denotes statistically significant difference at *p*-value ≤ 0.05.

3.2.2. Flexural strength evaluation

The present study compared the flexural strength of varying wt% of nanoZrO_2–SiO_2–HA to the control (Table 2). There was a linear correlation between the *FS* values and the wt% addition of nano powder to the GIC up to 7% following which further addition of 9% nanoZrO_2–SiO_2–HA to the GIC led to a decrease in the *FS*. These observations were in agreement with previous findings [32,70] and could be due to overcrowding of filler particles as well as dry cement mix owing to the high powder/liquid ratio needed to spatulate higher wt% nanoZrO_2–SiO_2–HA powder into the GIC. Arita and colleagues added HA granules at different weight (8–25%) percentages and concluded that HA addition to GIC at 8% had the highest *FS* values. In our study, similarly the highest *FS* values recorded were for GIC 5% nanoZrO_2–SiO_2–HA ~18.12 ± 13.88 MPa instead of GIC 9% nanoZrO_2–SiO_2–HA. Similar observations were made in another study in which the authors added HA and Si nano powder to cGIC at varying w/w% (5–20%) and reported the highest *FS* values of 17.68 ± 1.81 MPa for 10% GIC nanoHA–SiO_2. They concluded that further addition of higher percentages (15% and 20%) of nanoHA–SiO_2 to cGIC resulted in decreased *FS* values [43].

Table 2. Flexural strength comparison between the various experimental groups.

Group	Comparison	Mean flexural strength ± SD (MPa)	*p*-value
Control (14.38 ± 3.01 MPa)	GIC 3% nanoZrO_2–SiO_2–HA	14.44 ± 2.17	1.000
	GIC 5% nanoZrO_2–SiO_2–HA	18.12 ± 2.33*	0.000
	GIC 7% nanoZrO_2–SiO_2–HA	16.26 ± 2.93	0.148
	GIC 9% nanoZrO_2–SiO_2–HA	14.61 ± 2.55	0.999
GIC 3% nanoZrO_2–SiO_2–HA	GIC 5% nanoZrO_2–SiO_2–HA	18.12 ± 2.33*	0.000
	GIC 7% nanoZrO_2–SiO_2–HA	16.26 ± 2.93	0.171
	GIC 9% nanoZrO_2–SiO_2–HA	14.61 ± 2.55	1.000
GIC 5% nanoZrO_2–SiO_2–HA	GIC 7% nanoZrO_2–SiO_2–HA	16.26 ± 2.93	0.155
	GIC 9% nanoZrO_2–SiO_2–HA	14.61 ± 2.55	0.000
GIC 7% nanoZrO_2–SiO_2–HA	GIC 9% nanoZrO_2–SiO_2–HA	14.61 ± 2.55	0.258

*Denotes statistically significant difference at p-value ≤ 0.05.

In general, all the GIC nanoZrO_2–SiO_2–HA experimental groups had higher *FS* values than the control group. This is probably due to the toughening effect of ZrO_2 and additive effect of HA on the degree of polysalt bridge formation in the GIC matrix. Moreover, ZrO_2 does not dissolve in the distilled water upon immersion for extended periods [36].

There might be higher degrees of acid-base reaction within the structure of the setting cement due to presence of HA resulting in enhanced mechanical properties of GIC [72]. The addition of HA hastens the development of early *FS* of GIC in moist or wet conditions regardless of its form [32]. Another study, also reported a higher *FS* values when porous HA (~28%) was added to GIC as compared to control [73]. However, they reported *FS* of upto ~14 MPa which were much lower than the *FS* values recorded for GIC 5% nanoZrO_2–SiO_2–HA (18.12 ± 13.88 MPa) in our study.

The increase in FS of the GIC could also be due to the fact that the spherical nano Si particles occupy the voids present between the HA rods resulting in increased packing density in the GIC matrix, thereby, reducing crack propagation [34,41,43]. The GIC 5% nanoZrO_2–SiO_2–HA in our study exhibited the highest *FS* values by up to ~26% as compared to the control group 14.33 ± 3.01 MPa. Similarly, another study also reported the highest *FS* values at 5% addition of HA to GIC [70].

3.2.3. Surface roughness evaluation

In the present study, the average *Ra* values of SR for all tested GICs were within the range of 0.13–0.65 μm. The lowest SR were reported for GIC 3% nanoZrO_2–SiO_2–HA (0.13 ± 0.59 μm) and GIC 5% nanoZrO_2–SiO_2–HA (0.15 ± 0.29 μm) among the experimental groups (Table 3). The GIC 5% nanoZrO_2–SiO_2–HA group and control group had nearly identical SR profiles. These values from our study are in agreement with the findings of another recent study that reported the *SR* values (0.20 ± 0.07 μm) for a GIC carbomer which contains HA [74]. However, the *SR* profile of our material was smoother (0.15 ± 0.29 μm).

Table 3. Surface roughness comparison between the various experimental groups.

Group	Comparison	*Ra* value ± SD (μm)	*p*-value
Control (0.151 ± 0.019 μm)	GIC 3% nanoZrO_2–SiO_2–HA	0.13 ± 0.059	0.912
	GIC 5% nanoZrO_2–SiO_2–HA	0.15 ± 0.029	0.997
	GIC 7% nanoZrO_2–SiO_2–HA	0.33 ± 0.062*	0.000
	GIC 9% nanoZrO_2–SiO_2–HA	0.65 ± 0.051*	0.000
GIC 3% nanoZrO_2–SiO_2–HA	GIC 5% nanoZrO_2–SiO_2–HA	0.15 ± 0.029	0.762
	GIC 7% nanoZrO_2–SiO_2–HA	0.33 ± 0.062*	0.000
	GIC 9% nanoZrO_2–SiO_2–HA	0.65 ± 0.051*	0.000
GIC 5% nanoZrO_2–SiO_2–HA	GIC 7% nanoZrO_2–SiO_2–HA	0.33 ± 0.062*	0.000
	GIC 9% nanoZrO_2–SiO_2–HA	0.65 ± 0.051*	0.000
GIC 7% nanoZrO_2–SiO_2–HA	GIC 9% nanoZrO_2–SiO_2–HA	0.65 ± 0.051*	0.000

*Denotes statistically significant difference at p-value ≤ 0.05.

The highest Ra values were recorded for GIC 9% nanoZrO_2–SiO_2–HA (0.65 ± 0.05 μm) followed by GIC 7% nanoZrO_2–SiO_2–HA (0.33 ± 0.06 μm) and they were statistically different from the other groups. This suggests that the composition of the glass content may be responsible for these differences. As GIC 9% nanoZrO_2–SiO_2–HA had the highest filler content and since ZrO_2 is insoluble in the poly acid when compared to HA which dissolves easily, this probably was the reason for its increased *Ra*. Similarly, in another study, higher *Ra* values (0.64 μm) were reported for a silver-reinforced GIC, probably because silver particles are also insoluble in poly acids [75].

As mentioned previously, *SR* higher than 0.2 μm is likely to increase significantly bacterial adhesion, plaque maturation, thus increasing caries risk [76]. An increase in *SR* can result in alterations in the way light is reflected that in turn can make the material appear opaque. It has been reported that a surface may be considered reflective when its imperfections are well below 1 μm [77]. In this study, the GIC 5% nanoZrO_2–SiO_2–HA and GIC 3% nanoZrO_2–SiO_2–HA presented *SR* below 0.2 μm value without any efforts at polishing. Therefore, they can be considered to have an ideal surface profile.

4. Conclusion

The morphologic and microstructural characterization of the nanoZrO_2–SiO_2–HA synthesized by a modified one-pot synthesis followed by the evaluation of physico-mechanical properties revealed the following:

- TEM and SEM micrographs confirmed that all particles were in the nano-scale range with spherical ZrO_2 and SiO_2 particles embedded in the voids between rod-shaped HA crystallites.
- FTIR spectra confirmed the presence of functional groups corresponding to each element and the results of EDX and dot mapping revealed that these elements were evenly and homogenously dispersed throughout the sample with high density patterns visible for ZrO_2, Ca followed by P.
- The incorporation of nanoZrO_2–SiO_2–HA resulted in considerable improvement in the compressive and flexural strengths of cGIC. The GIC 5% nanoZrO_2–SiO_2–HA exhibited a

~30% and ~26% increase in compressive and flexural strength over cGIC, respectively. It also demonstrated surface roughness profile similar to that of cGIC.

Therefore, these nanoceramics can be considered as promising fillers for GIC to be used as a restorative dental material in high stress areas.

Acknowledgement

This research study was financially supported by Universiti Sains Malaysia under Research University Grant Scheme No. RUI 1001/PPSG/812164. The authors would like to acknowledge the expertise rendered by Prof. Ismail Ab Rahman, toward the research experiment design and preparation of this manuscript.

Conflict of interests

All authors declare no conflicts of interest in this paper.

References

1. Widstrom E, Birn H, Haugejorden O, et al. (1992) Fear of amalgam: dentists' experiences in the Nordic countries. *Int Dent J* 42: 65–70.
2. Pagano S, Chieruzzi M, Balloni S, et al. (2019) Biological, thermal and mechanical characterization of modified glass ionomer cements: the role of nanohydroxyapatite, ciprofloxacin and zinc l-carnosine. *Mat Sci Eng C-Mater* 94: 76–85.
3. Chieruzzi M, Pagano S, Lombardo G, et al. (2018) Effect of nanohydroxyapatite, antibiotic, and mucosal defensive agent on the mechanical and thermal properties of glass ionomer cements for special needs patients. *J Mater Res* 33: 638–649.
4. Wilson AD, Kent BE (1971) The glass-ionomer cement, a new translucent dental filling material. *J Appl Chem Biotechnol* 21: 313.
5. Wilson AD, Kent BE (1972) A new translucent cement for dentistry, the glass ionomer cement. *Brit Dent J* 132: 133–135.
6. Xie D, Brantley WA, Culbertson BM, et al. (2000) Mechanical properties and microstructures of glass-ionomer cements. *Dent Mater* 16: 129–138.
7. Anusavice KJ (2003) Mechanical properties of dental materials, *Philips Science of Dental Materials*, 11 Eds., Philadelphia: Saunders 48–67.
8. Bonifacio CC, Kleverlaan CJ, Raggio DP, et al. (2009) Physical-mechanical properties of glass ionomer cements indicated for atraumatic restorative treatment. *Aust Dent J* 54: 233–237.
9. Bonifacio CC, van Amerongen WE, Meschini TG, et al. (2010) Flowable glass ionomer cement as a liner: improving marginal adaptation of atraumatic restorative treatment restorations. *J Dent Child (Chic)* 77: 12–16.
10. Smith DC (1998) Development of glass-ionomer cement systems. *Biomaterials* 19: 467–478.

11. Smith DC (1968) A new dental cement. *Br Dent J* 124: 381–384.
12. Naasan MA, Watson TF (1998) Conventional glass ionomers as posterior restorations. A status report for the American Journal of Dentistry. *Am J Dent* 11: 36–45.
13. Oliva A, Della Ragione F, Salerno A, et al. (1996) Biocompatibility studies on glass ionomer cements by primary cultures of human osteoblasts. *Biomaterials* 17: 1351–1356.
14. Mount GJ (2002) *An Atlas of Glass Ionomer Cements: A Clinician's Guide*. United Kingdom: Martin Dunitz Ltd.
15. Six N, Lasfargues JJ, Goldberg M (2000) In vivo study of the pulp reaction to Fuji IX, a glass ionomer cement. *J Dent* 28: 413–422.
16. Dimkov A, Nicholson W, Gjorgievska E, et al. (2012) Compressive strength and setting time determination of glass-ionomer cements incorporated with cetylpyridinium chloride and benzalkonium chloride. *Prilozi* 33: 243–263.
17. McLean JW, Gasser O (1985) Glass-cermet cements. *Quintessence Int* 16: 333–343.
18. McLean J (1984) Alternatives to amalgam alloys: 1. *Br Dent J* 157: 432–433.
19. Sarkar NK (1999) Metal-matrix interface in reinforced glass ionomers. *Dent Mater* 15: 421–425.
20. Walls AW, Adamson J, McCabe JF, et al. (1987) The properties of a glass polyalkenoate (ionomer) cement incorporating sintered metallic particles. *Dent Mater* 3: 113–116.
21. Simmons JJ (1983) The miracle mixture. Glass ionomer and alloy powder. *Tex Dent J* 100: 6–12.
22. Simmons JJ (1990) Silver-alloy powder and glass ionomer cement. *J Am Dent Assoc* 120: 49–52.
23. Nourmohammadi J, Sadrnezhaad SK, Behnamghader A (2010) In vitro bioactivity of novel cured ionomer cement based on iron oxide. *Ceram Int* 36: 1645–1651.
24. Kerby R, Bleiholder R (1991) Physical properties of stainless-steel and silver-reinforced glass-ionomer cements. *J Dent Res* 70: 1358–1361.
25. Pamir T, Sen BH, Celik A (2005) Mechanical and fluoride release properties of titanium tetrafluoride-added glass-ionomer cement. *Dent Mater J* 24: 98–103.
26. Lohbauer U, Walker J, Nikolaenko S, et al. (2003) Reactive fibre reinforced glass ionomer cements. *Biomaterials* 24: 2901–2907.
27. Lohbauer U, Frankenberger R, Clare A, et al. (2004) Toughening of dental glass ionomer cements with reactive glass fibres. *Biomaterials* 25: 5217–5225.
28. Yamamoto Y (1984) Study on hydroxyapatite-polyacrylic acid composite cement (hydroxyapatite-glass ionomer cement). *Shika Zairyo Kikai* 3: 787–796.
29. Yap AU, Pek YS, Kumar RA, et al. (2002) Experimental studies on a new bioactive material: HAIonomer cements. *Biomaterials* 23: 955–962.
30. Moshaverinia M, Borzabadi-Farahani A, Sameni A, et al. (2016) Effects of incorporation of nano-fluorapatite particles on microhardness, fluoride releasing properties, and biocompatibility of a conventional glass ionomer cement (GIC). *Dent Mater J* 35: 817–821.
31. Mitra SB, Wu D, Holmes BN (2003) An application of nanotechnology in advanced dental materials. *J Am Dent Assoc* 134: 1382–1390.

32. Arita K, Lucas ME, Nishino M (2003) The effect of adding hydroxyapatite on the flexural strength of glass ionomer cement. *Dent Mater J* 22: 126–136.
33. Arita K, Yamamoto A, Shinonaga Y, et al. (2011) Hydroxyapatite particle characteristics influence the enhancement of the mechanical and chemical properties of conventional restorative glassionomer cement. *Dent Mater J* 30: 672–683.
34. Shiekh RA, Ab Rahman I, Luddin N (2014) Modification of glass ionomer cement by incorporating hydroxyapatite-silica nano-powder composite: sol-gel synthesis and characterization. *Ceram Int* 40: 3165–3170.
35. Rahman IA, Masudi SAM, Luddin N, et al. (2014) One-pot synthesis of hydroxyapatite-silica nanopowder composite for hardness enhancement of glass ionomer cement (GIC). *B Mater Sci* 37: 213–219.
36. Gu YW, Yap AU, Cheang P, et al. (2005) Effects of incorporation of HA/ZrO_2 into glass ionomer cement (GIC). *Biomaterials* 26: 713–720.
37. Gu YW, Yap AUJ, Cheang P, et al. (2005) Developement of zirconia–glass ionomer cement composites. *J Non-Cryst Solids* 351: 508–514.
38. Rajabzadeh G, Salehi S, Nemati A, et al. (2014) Enhancing glass ionomer cement features by using the HA/YSZ nanocomposite: a feed forward neural network modelling. *J Mech Behav Biomed Mater* 29: 317–327.
39. Silva VV, Lameiras FS, Lobato ZI (2002) Biological reactivity of zirconia-hydroxyapatite composites. *J Biomed Mater Res* 63: 583–590.
40. Chou BY, Chang E (2002) Plasma-sprayed hydroxyapatite coating on titanium alloy with ZrO_2 second phase and ZrO_2 intermediate layer. *Surf Coat Tech* 153: 84–92.
41. Rahman IA, Ghazali NAM, Bakar WZW, et al. (2017) Modification of glass ionomer cement by incorporating nanozirconia-hydroxyapatite-silica nano-powder composite by the one-pot technique for hardness and aesthetics improvement. *Ceram Int* 43: 13247–13253.
42. Panda R, Hsieh M, Chung R, et al. (2003) FTIR, XRD, SEM and solid state NMR investigations of carbonate-containing hydroxyapatite nano-particles synthesized by hydroxide-gel technique. *J Phys Chem Solids* 64: 193–199.
43. Moheet IA, Luddin N, Ab Rahman I, et al. (2018) Evaluation of mechanical properties and bond strength of nano-hydroxyapatite-silica added glass ionomer cement. *Ceram Inte* 44: 9899–9906.
44. Perez Cdos R, Hirata RJ, da Silva AH, et al. (2009) Effect of a glaze/composite sealant on the 3-D surface roughness of esthetic restorative materials. *Oper Dent* 34: 674–680.
45. Takei T, Kato K, Meguro A, et al. (1999) Infrared spectra of geminal and novel triple hydroxyl groups on silica surface. *Colloid Surface A* 150: 77–84.
46. Rahman I, Masudi SaM, Luddin N, et al. (2013) One-pot synthesis of hydroxyapatite-silica nano-powder composite for hardness enhancement of glass ionomer cement (GIC). *B Mater Sci* 37: 213–219.
47. Zhan Z, Zeng HC (1999) A catalyst-free approach for sol-gel synthesis of highly mixed ZrO_2–SiO_2 oxides. *J Non-Crys Solids* 243: 26–38.

48. Fernando MS, de Silva RM, de Silva KMN (2015) Synthesis, characterization, and application of nano hydroxyapatite and nanocomposite of hydroxyapatite with granular activated carbon for the removal of Pb^{2+} from aqueous solutions. *Appl Surf Sci* 351: 95–103.
49. Wang A, Liu D, Yin H, et al. (2007) Size-controlled synthesis of hydroxyapatite nanorods by chemical precipitation in the presence of organic modifiers. *Mat Sci Eng C-Mater* 27: 865–869.
50. Singh AK, Nakate UT (2014) Microwave synthesis, characterization, and photoluminescence properties of nanocrystalline zirconia. *Sci World J* 2014: 349457.
51. Ranjbar M, Yousefi M, Lahooti M, et al. (2012) Preparation and characterization of tetragonal zirconium oxide nanocrystals from isophthalic acid-zirconium(IV) nanocomposite as a new precursor. *Int J Nanosci Nanotechno* 8: 191–196.
52. Xiao Y, Li D, Fan H, et al. (2007) Preparation of nano-HA/PLA composite by modified-PLA for controlling the growth of HA crystals. *Mater Lett* 61: 59–62.
53. Nejati E, Mirzadeh H, Zandi M (2008) Synthesis and characterization of nano-hydroxyapatite rods/poly(L-lactide acid) composite scaffolds for bone tissue engineering. *Compos Part A-Appl S* 39: 1589–1596.
54. Stoch A, Jastrzębski W, Brożek A, et al. (2000) FTIR absorption-reflection study of biomimetic growth of phosphates on titanium implants. *J Mol Struct* 555: 375–382.
55. de Bruijn JD, Bovell YP, van Blitterswijk CA (1994) Structural arrangements at the interface between plasma sprayed calcium phosphates and bone. *Biomaterials* 15: 543–550.
56. Jafarzadeh M, Rahman IA, Sipaut CS (2009) Synthesis of silica nanoparticles by modified sol-gel process: the effect of mixing modes of the reactants and drying techniques. *J Sol-Gel Sci Techn* 50: 328–336.
57. Rahman IA, Vejayakumaran P, Sipaut CS, et al. (2007) An optimized sol-gel synthesis of stable primary equivalent silica particles. *Colloid Surface A* 294: 102–110.
58. Moheet IA, Luddin N, Ab Rahman I, et al. (2018) Evaluation of mechanical properties and bond strength of nano-hydroxyapatite-silica added glass ionomer cement. *Ceram Int* 44: 9899–9906.
59. Gu YW, Yap AUJ, Cheang PHN, et al. (2005) Zirconia-glass ionomer cement-a potential substitute for miracle mix. *Scripta Mater* 52: 113–116.
60. Anusavice KJ (2003) Mechanical properties of dental materials, In: Anusavice KJ, Shen C, Rawls HR, Philips Science of Dental Materials, 11 Eds., New York: Saunders, 48–67.
61. Takaki P, Vieira M, Bommarito S (2014) Maximum bite force analysis in different age groups. *Int Arch Otorhinolaryngol* 18: 272–276.
62. Rios D, Honório HM, Araújo PAd, et al. (2002) Wear and superficial roughness of glass ionomer cements used as sealants, after simulated toothbrushing. *Pesqui Odontol Bras*16: 343–348.
63. Yip HK, Lam WT, Smales RJ (1999) Fluoride release, weight loss and erosive wear of modern aesthetic restoratives. *Br Dent J* 187: 265–270.
64. Yip HK, Lam WT, Smales RJ (1999) Surface roughness and weight loss of esthetic restorative materials related to fluoride release and uptake. *J Clin Pediatr Dent* 23: 321–326.

65. Yip KH, Peng D, Smales RJ (2001) Effects of APF gel on the physical structure of compomers and glass ionomer cements. *Oper Dent* 26: 231–238.
66. Mount GJ (1995) Some physical and biological properties of glass ionomer cement. *Int Dent J* 45: 135–140.
67. Lucas ME, Arita K, Nishino M (2003) Toughness, bonding and fluoride-release properties of hydroxyapatite-added glass ionomer cement. *Biomaterials* 24: 3787–3794.
68. Cales B, Stefani Y, Lilley E (1994) Long-term in vivo and in vivo aging of a zirconia ceramic used in orthopaedy. *J Biomed Mater Res* 28: 619–624.
69. Uo M, Sjoren G, Sundh A, et al. Cytotoxicity and bonding property of dental ceramics. *Dent Mater* 19: 487–492.
70. Moshaverinia A, Ansari S, Moshaverinia M, et al. (2008) Effects of incorporation of hydroxyapatite and fluoroapatite nanobioceramic into conventional galss ionomer cements. *Acta Biomater* 4: 432–440.
71. Piconi C, Maccauro G (1999) Zirconia as a ceramic biomaterial. *Biomaterials* 20: 1–25.
72. Aoki H (1991) *Science and Medical Applications of Hydroxyapatite*. Tokyo: JAAS.
73. Shinonaga Y, Arita K, Nishimura T, et al. (2015) Effects of porous-hydroxyapatite incorporated into glass-ionomer sealants. *Dent Mater J* 34: 196–202.
74. Lopes CMCF, Galvan J, Chibinski ACR, et al. (2018) Fluoride release and surface roughness of a new glass ionomer cement: glass carbomer. *Rev Odontol UNESP* 47: 1–6.
75. Bala O, Arisu HD, Yikilgan I, et al. (2012) Evaluation of surface roughness and hardness of different glass ionomer cements. *Eur J Dent* 6: 79–86.
76. Bollen CM, Lambrechts P, Quirynen M (1997) Comparison of surface roughness of oral hard materials to the threshold surface roughness for bacterial plaque retention: a review of the literature. *Dent Mater* 13: 258–269.
77. Warren DP, Colescott TD, Henson HA, et al. (2002) Effects of four prophylaxis pastes on surface roughness of a composite, a hybrid ionomer, and a compomer restorative material. *J Esthet Restor Den* 14: 245–251.

AIMS Press

© 2019 the Author(s), licensee AIMS Press. This is an open access article distributed under the terms of the Creative Commons Attribution License (http://creativecommons.org/licenses/by/4.0)